



Design, synthesis and investigation of potential anti-inflammatory activity of O-alkyl and O-benzyl hesperetin derivatives

Ai-Ling Huang^{a,b,c}, Yi-Long Zhang^{a,b,c,1}, Hai-Wen Ding^{a,b,c}, Bo Li^{a,b,c}, Cheng Huang^{a,b,c}, Xiao-Ming Meng^{a,b,c}, Jun Li^{a,b,c,*}

^a The Key Laboratory of Major Autoimmune Diseases, Anhui Institute of Innovative Drugs, School of Pharmacy, Anhui Medical University, People's Republic of China

^b The Key Laboratory of Anti-inflammatory of Immune medicines, Ministry of Education, People's Republic of China

^c Institute for Liver Diseases of Anhui Medical University, People's Republic of China

ARTICLE INFO

Keywords:

Hesperetin derivatives
Synthesis
Anti-inflammatory activity
NF- κ B
Structure-activity relationships
Molecular docking

ABSTRACT

Hesperetin has been known to exert several activities such as anti-oxidant, antitumor and anti-inflammatory. To find hesperetin derivatives showing better activity, sixteen novel hesperetin derivatives were designed and synthesized. The new obtained compounds were investigated for their anti-inflammatory activity by inhibiting interleukin-1 β (IL-1 β), interleukin-6 (IL-6) and production of nitric oxide (NO) in mouse RAW264.7 macrophages, and the structure-activity relationship of them was discussed. Among them, the compound **11**, **2c** demonstrated more effective inhibitory activity of IL-1 β and IL-6, meanwhile, the compound **11** showed the best inhibition of NO production. The results of NO inhibition study were basically accord with the molecular docking results of inducible nitric oxide synthase (iNOS). Furthermore, the expression of LPS-induced iNOS and components of NF- κ B signaling pathway were reduced by compound **11**. Our results suggest that the inhibitory effect of compound **11** on LPS-stimulated inflammatory mediator production in RAW 264.7 cells is associated with the suppression of NF- κ B signaling pathway and inhibition of iNOS protein and iNOS activity. From *in vivo* study, it was also observed that compound **11** had hepato-protective and anti-inflammatory effects in CCl₄-induced acute liver injury mouse models.

1. Introduction

In Chinese Traditional Medicine, Citrus is the fruit peel of the Rutaceae plants that produce oranges (*Citrus reticulata* Blanco) and its cultivars. Hesperetin and hesperedin are the primary active contents of citrus fruits. [1] Flavonoids represent a class of polyphenolic compounds found in plants, such as fruit, vegetables, tea and soybeans, which are generally stored as glycosides because they are more stable than their aglycones [2,3]. However, due to their poor bioavailability, glycosides are hydrolyzed to aglycones to be used [4]. Hesperedin is a flavanone glycoside, consisting of an aglycone (hesperetin) and an attached disaccharide (rutinose) [5]. As a result, hesperedin has a lower bioavailability than hesperetin because of the rutinose moiety attached to the flavonoid and orally ingested hesperedin is hydrolyzed to hesperetin in the gastrointestinal tract and conjugated during absorption [6].

Hesperetin and its derivatives have been found to possess a wide range of pharmacological properties, including anti-hyperglycemic

[5,7], anti-tumor and anti-cardiovascular [8,9], antioxidant, anti-inflammatory [10] and antihypertensive [11] activities. The biological activities depend remarkably on compounds' structural characteristics such as conjugations, degree of hydroxylation and substitutions [12]. Because hesperetin belongs to polyphenols, various functional groups can be substituted for its phenyl groups [2]. Notably, a small alternation in the chemical structure of flavonoids may lead to significant changes in biological activities. We have previously studied that 5, 7, 3'-triacetyl hesperetin could suppress adjuvant-induced arthritis (AA) in rats through modulating JAK2/STAT3 pathway, while 7, 3'-dimethoxy hesperetin inhibited inflammation by inducing synovial apoptosis in AA rats [13]. Then we found hesperetin derivative-7 inhibited the activation and proliferation of PDGF-BB-induced HSC-T6 and attenuated liver fibrosis through targeting the Wnt/ β -catenin signaling pathway [14], while hesperetin derivative 11 suppressed hepatic stellate cell activation and proliferation by targeting PTEN/AKT pathway [15]. Based on this, we tried to prepare compounds derivatized at 7-position, which may facilitate the design of more potent hesperetin derivatives as anti-

* Corresponding author at: School of Pharmacy, Anhui Medical University, Hefei, Anhui 230032, People's Republic of China.

E-mail addresses: huangcheng812@ahmu.edu.cn (C. Huang), lj@ahmu.edu.cn (J. Li).

¹ This author contributes equally to the first author

inflammatory leads.

In the inflammation processes, the expression of cytokines or mediators such as tumor necrosis factor- α (TNF- α), interleukin-1 β (IL-1 β), and interleukin-6 (IL-6), as well as nitric oxide synthase are induced in immune cells by lipopolysaccharide (LPS) and interferon- γ (IFN- γ). The suppression of cytokines production is an indicator of anti-inflammatory agents. NO plays an important physiological role as a defense molecule in the immune system, while the excess production of NO by macrophages contributes to numerous pathological processes [16]. Inducible nitric oxide synthase (iNOS), which is responsible for the overproduction of NO, has been involved in a number of inflammatory diseases. Therefore, selective inhibition of iNOS would be a valid approach and prime target for the reduction of inflammation [17]. On the other hand, NF- κ B represents a group of structurally related and evolutionarily conserved proteins that are responsible for the regulation of the expression of several genes involved in inflammatory response [18,19]. NF- κ B is a major transcription factor that modulates the expression of pro-inflammatory proteins (e.g., iNOS) and pro-inflammatory cytokines (e.g., TNF- α and IL-1 β) induced by LPS. Several studies have indicated the contribution of components of the NF- κ B signaling pathways in the pathogenesis of chronic inflammatory disease [20].

Herein, we report on synthesis and inhibitory activity on expression of IL-1 β and IL-6, iNOS and consequent production of NO, a representative mediator of inflammatory responses, in the LPS stimulated RAW 264.7 macrophage cell line of novel hesperetin derivatives. Furthermore, we investigated the suppression of NF- κ B signaling pathway by the candidate. For the *in vivo* study, the potential candidate demonstrated a remarkable hepato-protective effect in CCl₄-induced acute liver injury as expected. In addition, according to our speculation, we did a supplementary molecular docking between compounds and iNOS at the end of the study, which finally found that the docking scores were essentially correspond with the *in vitro* study. The further investigation is in progress. The goal of this study was to find hesperetin derivatives showing better biological activity than hesperetin itself. Analysis of the structure-activity relationship of the derivatives may provide a way to develop novel anti-inflammatory drug candidates.

2. Result and discussion

2.1. Chemistry

The preparation of a series of novel hesperetin derivatives was carried out as illustrated in Scheme 1. The compounds differed in the substitution of the 7-hydroxyl. The derivatives of the title compounds were prepared by reacting with different brominated aryl and alkyl to obtain **1a–1m** and **2a–2c**. The choice of the reaction is at a hydroxyl group, which means at the 7-position or/and 3'-position. During the stirring, appropriate and slight K₂CO₃ was intermittently added to the solution so that the nucleophilic substitution could act or only act at the 7-position as far as possible. The structures of compounds were confirmed by elemental and spectral analyses. Analytical and spectral data (¹H NMR, ¹³C NMR and mass spectra) of the synthesized compounds were in full agreement with the proposed structures.

2.2. *In vitro* pharmacology

2.2.1. Cytotoxicity and cell viability test

MTT assay was carried out to evaluate cytotoxicity and cell viability of hesperetin derivatives. The cytotoxicity tests were performed at the concentration of 400 μ M, 200 μ M, 100 μ M, 50 μ M, and 25 μ M, and the results are shown in Table 1. According to the IC₅₀ values, the concentrations of the cell viability tests were designed at 40 μ M, 20 μ M, 10 μ M, and 5 μ M. The results clearly demonstrate that after the concentration of 20 μ M treatment, the cell viability of several compounds are < 90%. Nevertheless, at the concentration of 10 μ M as shown in

Table 1, most of these compounds are not significantly cytotoxic. Thereby, further studies for the anti-inflammatory activity with the compounds were observed at the test concentration of 10 μ M.

2.2.2. Inhibitory activity of NO production

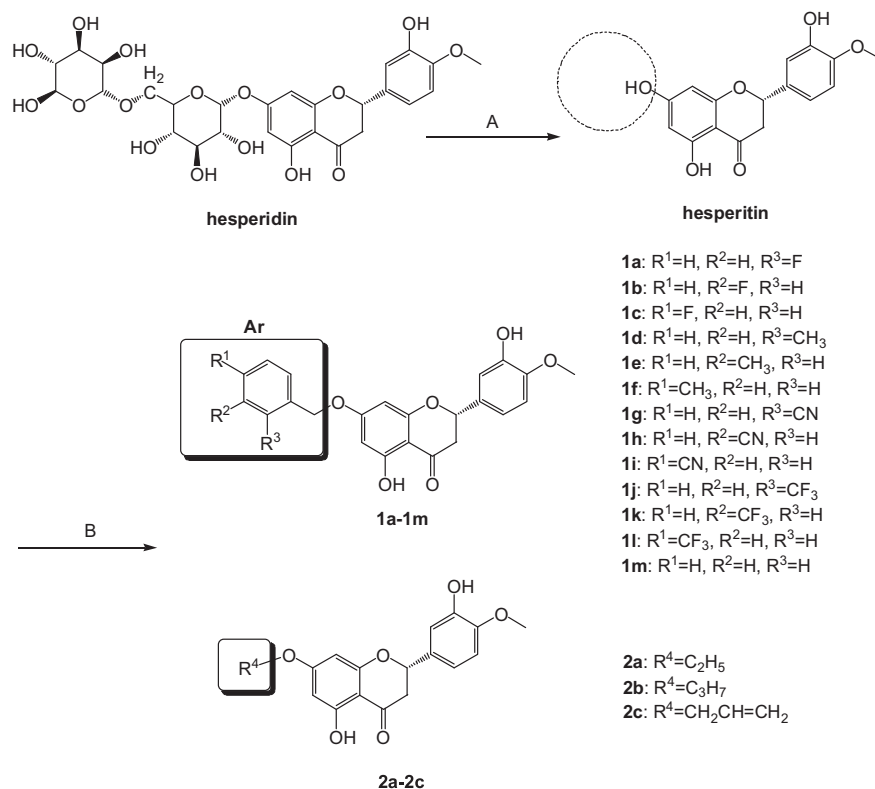
Macrophages produce various pro-inflammatory mediators, including the short-lived free radical NO. Moreover, LPS is one of the most powerful activators of macrophages and stimulates NO production. First of all, the compounds had been confirmed to have no cytotoxic activity toward RAW264.7 cells at the concentration of 10 μ M. Thereby, the inhibition of NO production by compounds was not attributable to cytotoxic effects at the test concentration. The synthetic hesperetin derivatives were evaluated for inhibitory effects on the production of NO in LPS stimulated RAW264.7 macrophage cells. When the cells were treated with LPS (1 μ g/mL) for 22 h, the NO production was markedly stimulated from the basal level of $1.095 \pm 0.056 \mu$ M to $19.908 \pm 0.898 \mu$ M. The inhibitory activity of the compounds is summarized in Table 2. LPS stimulation resulted in a marked induction of NO production as compared to untreated cells. In addition, pretreatment with some of these compounds prior to LPS stimulation significantly reduced NO production. Among them, compound **1f**, **1h**, **1i** and **1k** showed great activities, while compound **1l** exhibited the best inhibitory effect. Meanwhile, compound **1l** inhibited production of NO in 37.30% at the concentration of 10 μ M.

2.2.3. Inhibitory activity of IL-1 β and IL-6

The anti-inflammatory activity of hesperetin and its derivatives were also evaluated by their inhibitory effect against LPS-induced IL-1 β and IL-6 release in the RAW264.7 macrophages. The results are summarized in Fig. 1 and expressed as percent of LPS control. IL-1 β and IL-6 secretion was significantly inhibited by most of the synthetic compounds at the concentration of 10 μ M. The inhibition rates were from 40.12% to 91.72% and from 45.94% to 89.37%, respectively. Half of the synthetic hesperetin derivatives such as compound **1h**, **1k**, **1l**, **2a**, **2b** and **2c**, had greater inhibitory effects than hesperetin itself. Though the activities of some compounds were somewhat low in comparison with hesperetin, the remainder tested compounds significantly inhibited LPS-induced expression of both IL-1 β and IL-6. What's more, compound **1l** can efficiently block the LPS-induced production of different cytokines in macrophages, which is in good agreement with our observations of its activity in NO inhibition. Therefore, compound **1l** was selected for further pharmacological evaluations.

2.2.4. Analysis of structure-activity relationship

Wen-Jun Jiang et al. [21] have discussed that the suppression of NO production of flavonoids is related to the overall topology of the molecules as well as the electrostatic property of the B ring. However, the impact on the biological activity of the 7-position could be observed according to Table 2. Comparing compound **1m** with other benzyl substituted hesperetin derivatives, the presence of an electron-withdrawing group on the benzyl group is important for the inhibition of NO production. Compounds with the cyanobenzyl group or trifluoromethylbenzyl group are generally better inhibitors than those of the fluorobenzyl group or methylbenzyl group. That is, compounds that introduce an electron-withdrawing group on the 7-benzyl ring generally have higher activities than compounds substituted with an electron donor group. The result can also be obtained from the inhibitory effect of IL-1 β and IL-6 release shown in Fig. 1. Besides, the carbon in the cyano group and the fluorine in the trifluoromethyl group have lone pair electrons, which theoretically can form hydrogen bonds to enhance the binding capacity of the compound to receptors. Furthermore, from the comparison between electron-withdrawing groups, it can be found that the attachment of the group to the benzyl group also affects the biological activities. Compound **1h** (meta-position), **1k** (meta-position), and **1l** (para-position) remarkably suppressed the NO production and the release of IL-1 β and IL-6 at the same time. In contrast, compound



Scheme 1. Synthesis of hesperetin derivatives **1a–1m** and **2a–2c**. Reagents and conditions: (A) 96% H₂SO₄, MeOH, 80 °C, reflux. (B) DMF, K₂CO₃, Bromide, 20 °C.

Table 1

IC₅₀ value and cell viability of RAW 264.7 cells at the compound concentration of 20 μM and 10 μM.

Compound	IC ₅₀ (μM)	%cell viability in 20 μM	%cell viability in 10 μM
1a	185.66 ± 1.96	83.08 ± 4.51	89.45 ± 2.11
1b	287.28 ± 4.34	83.96 ± 0.81	90.89 ± 1.78
1c	245.13 ± 1.33	82.77 ± 2.71	89.29 ± 0.99
1d	291.05 ± 8.13	92.11 ± 2.23	102.33 ± 5.78
1e	216.10 ± 5.97	89.70 ± 0.36	91.00 ± 0.15
1f	266.44 ± 2.99	98.43 ± 1.96	102.50 ± 3.84
1g	249.38 ± 5.28	87.71 ± 3.18	98.50 ± 4.05
1h	208.75 ± 8.58	100.95 ± 0.81	101.62 ± 0.97
1i	131.60 ± 2.34	95.08 ± 1.20	102.52 ± 1.78
1j	120.14 ± 2.27	103.02 ± 1.09	98.41 ± 0.46
1k	128.01 ± 1.14	79.63 ± 1.54	88.34 ± 2.59
1l	148.87 ± 1.44	80.31 ± 0.09	92.85 ± 3.86
1m	177.35 ± 1.14	89.95 ± 0.23	92.05 ± 2.91
2a	229.34 ± 4.00	112.59 ± 2.06	106.47 ± 0.34
2b	158.73 ± 2.64	92.93 ± 1.13	91.93 ± 1.10
2c	158.45 ± 3.98	98.32 ± 2.78	96.94 ± 2.20

The results are presented as the means ± SD of three different experiments.

2a, **2b**, and **2c**, which had potential inhibitory effect of IL-1β and IL-6 release, demonstrated no NO inhibition. The mechanism of the two different series of derivatives needs further investigation.

2.2.5. Effect of compound **1l** on iNOS and NF-κB pathway

High levels of NO are considered to be a biomarker for inflammatory disorders and a useful target for the procurement of anti-inflammatory agents [22]. The overproduction of NO can attribute to the overexpression of iNOS which is significant in inflammatory processes. The iNOS protein level was markedly increased in LPS-induced RAW264.7 cells (Fig. 2), but co-treatment with compound **1l** suppressed the iNOS protein level in a concentration-dependent manner. This finding suggests that the inhibition of NO production by compound **1l** may be correlated with its suppressive effect on LPS-induced iNOS

Table 2

NO production in LPS-treated RAW264.7 cells at the compound concentration of 10 μM.

Compound	NO production(μM)
LPS	19.908 ± 0.898
DMSO	1.095 ± 0.056
Hesperetin	18.056 ± 0.099*
1a	19.702 ± 0.836
1b	16.184 ± 0.108**
1c	17.803 ± 0.218*
1d	15.666 ± 0.295**
1e	17.612 ± 0.183*
1f	15.418 ± 0.193**
1g	16.364 ± 0.113**
1h	14.107 ± 0.143***
1i	14.986 ± 0.191***
1j	18.086 ± 0.277*
1k	14.465 ± 0.316***
1l	12.892 ± 0.261****
1m	19.39 ± 0.193
2a	18.132 ± 0.145*
2b	17.729 ± 1.178*
2c	19.911 ± 0.267

The LPS and DMSO group were pretreated with 1% DMSO solution without compound. The test compounds (10 μM) were 2 h prior to LPS stimulation. Data are presented as mean ± SD (n = 3) and analyzed using Dunnett-t-test compared to vehicle. The difference was considered statistically significant when p (*) < 0.05, (**) < 0.01, (***) < 0.001, (****) < 0.0001.

protein.

The translocation of NF-κB to the nucleus is preceded by the phosphorylation and proteolytic degradation of IκBα by IκB kinases (IKKs) [23]. In general, in un-stimulated cells, NF-κB subunits (p50 and/or p65) form a complex with an inhibitory factor, IκBα, in the cytosol and thus are inactivated. [22] When stimulated by pro-inflammatory

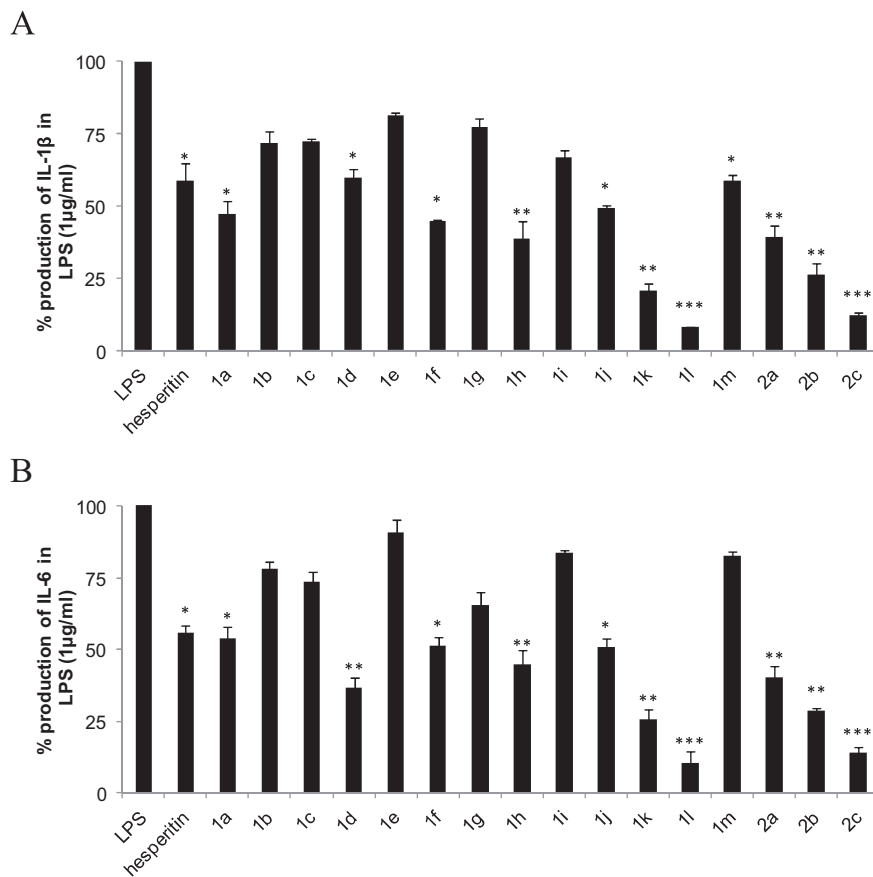


Fig. 1. Hesperetin and synthetic compounds inhibited LPS-induced IL-1 β and IL-6 secretion in RAW 264.7 macrophages. Cells were pretreated with synthetic compounds (10 μ M) for 2 h, then treated with LPS (1 μ g/ml) for 22 h. The results are expressed as percent of LPS control. Data are presented as mean \pm SD ($n = 3$) and analyzed using Dunnett- t -test. The difference was considered statistically significant when p (*) < 0.05, (**) < 0.01, (***) < 0.001.

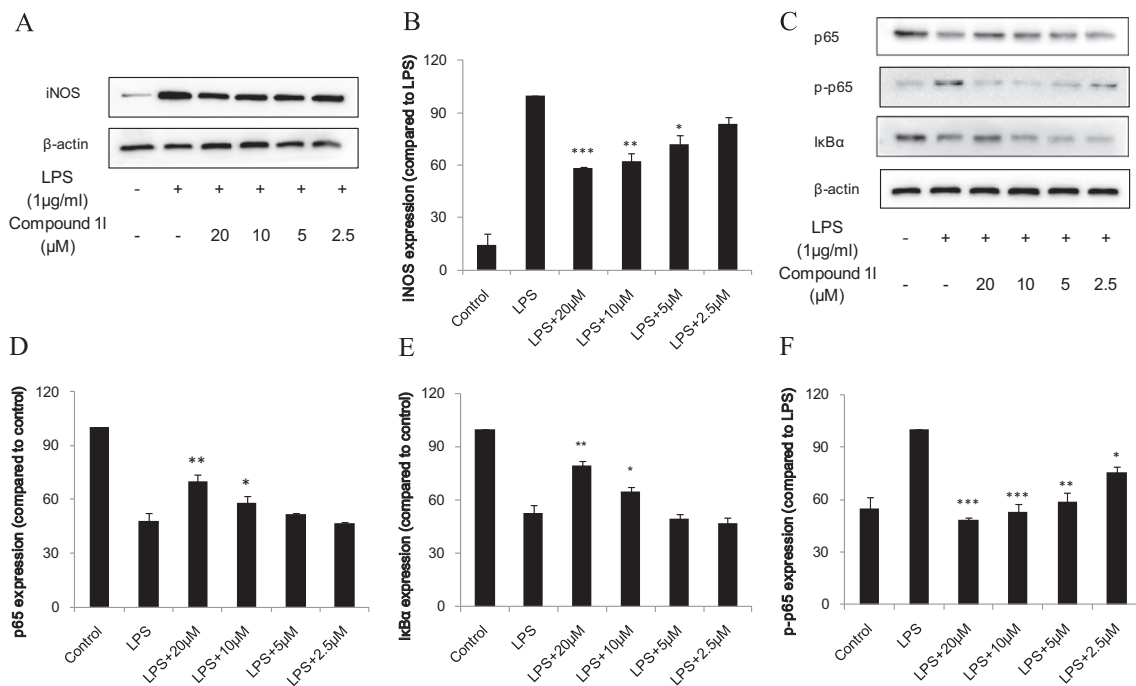


Fig. 2. The effects of compound 11 on iNOS, NF- κ B and its related proteins. RAW 264.7 cells were pretreated with various concentrations of compound 11 for 2 h and then stimulated with LPS (1 μ g/mL) for 1 h (p-p65) or 22 h (iNOS, p65, I κ B α). Proteins were analyzed using western blotting. (B) Quantitative analysis of iNOS expression, β -actin was used as loading control; (D) Quantitative analysis of p65 expression, β -actin was used as loading control; (E) Quantitative analysis of I κ B α expression, β -actin was used as loading control; (F) Quantitative analysis of p-p65 expression, β -actin was used as loading control. Data are presented as means \pm SD ($n = 3$). * p < 0.05, ** p < 0.01, *** p < 0.001 versus the LPS (treated with LPS only) group.

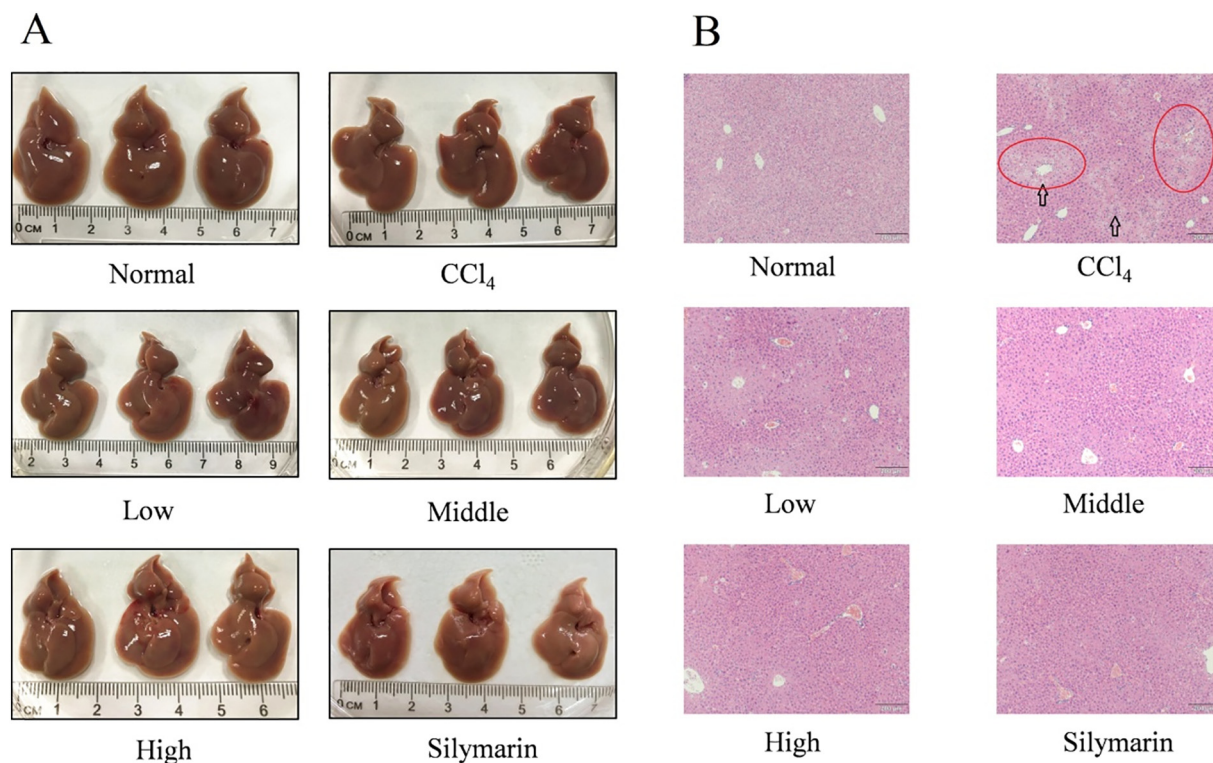


Fig. 3. Hepato-protective effects of compound 11 on mice with CCl_4 -induced acute liver injury model, $n = 8$ mice per group. (A) Representative images from C57BL/6J mice fresh livers in Control, CCl_4 , compound 11 treatment groups and Silymarin treatment group. (B) Pathology observation of mice liver tissues sections stained with hematoxylin and eosin (H & E). Representative views from each group are presented ($\times 10$). Low: compound 11 (50 mg/kg) + CCl_4 ; Middle: compound 11 (100 mg/kg) + CCl_4 ; High: compound 11 (200 mg/kg) + CCl_4 .

signaling, $\text{I}\kappa\text{B}\alpha$ is phosphorylated by IKKs and then subject to ubiquitin-mediated degradation. In NF- κB signaling, $\text{I}\kappa\text{B}$ degradation frees NF- κB p65 subunit and allows it to translocate to the nucleus, followed by turning on transcription of inflammatory genes [24]. As shown in Fig. 2, LPS induced the $\text{I}\kappa\text{B}\alpha$ degradation and the phosphorylation of p65. A pretreatment with compound 11 significantly reversed LPS-induced degradation of $\text{I}\kappa\text{B}\alpha$, further showed dose-dependent inhibition against LPS-induced $\text{I}\kappa\text{B}\alpha$ degradation. A similar result was also observed in inhibition on p65 phosphorylation in a dose-dependent manner. Thus, compound 11 seems to exert anti-inflammatory actions partly via inhibiting NF- κB pathway.

We have previously demonstrated that several hesperetin derivatives affected iNOS protein and Notch signaling [6]. These results indicate a mechanistic difference among active anti-inflammatory hesperetin derivatives, although they are derived from the same structural lead. This suggests that the structural modification increases and even changes or has different possible molecular targets. It is really worthy to be further investigated in the future for the chemical and structural features influencing the biological mechanism.

2.3. In vivo anti-inflammatory activity

2.3.1. Effects of compound 11 on histopathological changes in the liver tissue of CCl_4 -induced acute liver injury mice

In Fig. 3, histopathological study was performed to investigate the effect of compound 11 on mice with CCl_4 -induced acute liver injury. Mice liver tissues sections stained with hematoxylin and eosin (H & E) showed that CCl_4 (1%) injection caused remarkable acute liver injury exhibited hepatocyte necrosis, irregularly arranged, vacuole formation, loss of cellular boundaries and inflammatory cells infiltration compared with the control group. Notably, after the compound 11 of different concentrations (50 mg/kg, 100 mg/kg, 200 mg/kg) and Silymarin (200 mg/kg) treatment, the histological features of hepatocytes were

restored to some extent compared with the control group. High-dose compound 11 (200 mg/kg) yielded more effective rescue, almost comparable to positive control group.

2.3.2. Effects of compound 11 on hepatic markers and cytokine production in the CCl_4 -induced acute liver injury model

ALT, AST, are liver enzyme markers, and elevated levels of these markers in serum indicate the loss of hepatocyte structural integrity and liver injury [25]. Compared their levels with the control group, AST, ALT levels were significantly increased in mice in the CCl_4 group ($p < 0.001$), as shown in Fig. 4A and B. However, mice treated with compound 11 (50 mg/kg, 100 mg/kg, 200 mg/kg) and Silymarin (200 mg/kg) markedly attenuated the serum levels of ALT and AST in a dose-dependent manner. Moreover, results of ELISA assay demonstrated that compound 11 pretreatment significantly attenuated pro-inflammatory cytokines IL-1 β and IL-6 secretion levels in a concentration-dependent manner (Shown in Fig. 4C and D). Additionally, the compound 11 treatment group (200 mg/kg) showed similar hepatoprotective and anti-inflammatory effects compared with Silymarin (200 mg/kg) group. All the features indicate that compound 11 has significant effects on hepato-protective and suppresses the inflammatory response in CCl_4 -induced acute liver injury.

2.4. Molecular docking

Molecular docking simulations have become an important tool for understanding the interaction mode and the structure-activity relationships of ligands with receptors [1]. Indeed, targeting the iNOS has been proposed as an anti-inflammatory therapeutic strategy since high concentrations of NO are essential in inflammation and related processes [26]. It has been reported that the anti-inflammatory effect of lots of natural products and their derivatives was associated with the active site of iNOS. Although our results have verified the iNOS

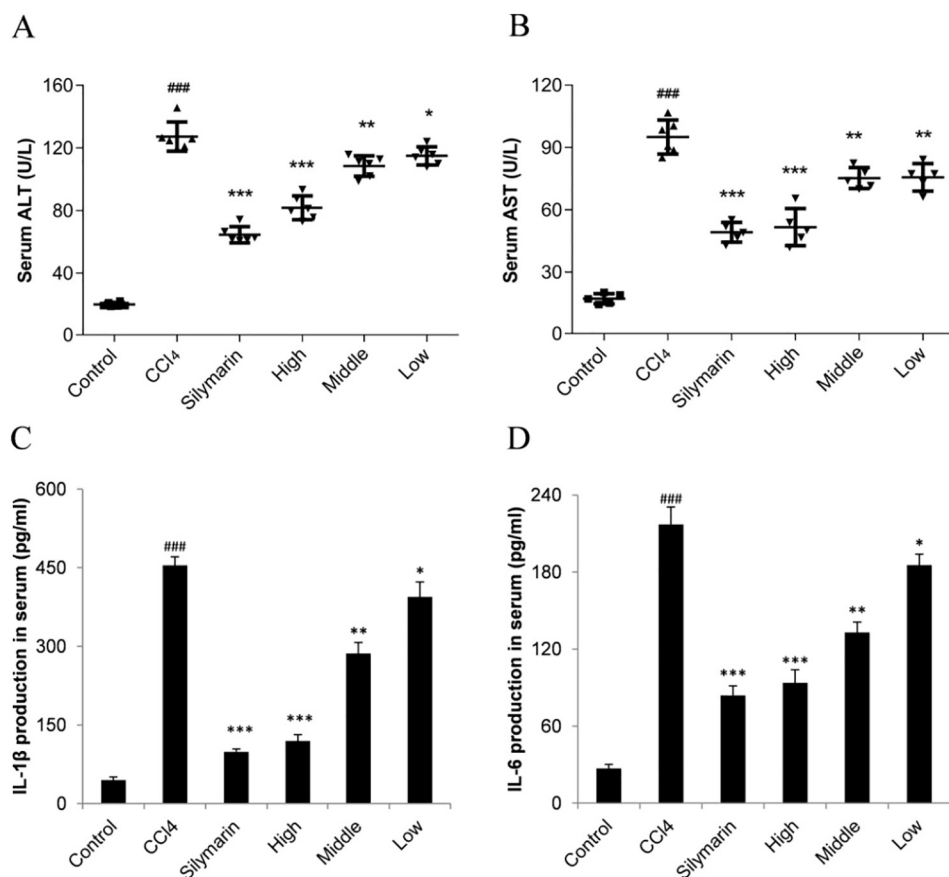


Fig. 4. Effects of compound 11 on hepatic markers and cytokine production in the CCl₄-induced acute liver injury model. (A) Effect of different concentrations of compound 11 and Silymarin on serum ALT level of each group. (B) Effect of different concentrations of compound 11 and Silymarin on serum AST level of each group. (C) Effect of different concentrations of compound 11 and Silymarin on serum IL-1 β level of each group. (D) Effect of different concentrations of compound 11 and Silymarin on serum IL-6 level of each group. Data represent the mean \pm S.D. for at least three independent experiments. * p < 0.05, ** p < 0.01, *** p < 0.001 versus the CCl₄ (treated with CCl₄ only) group. # p < 0.05, ## p < 0.01, ### p < 0.001 versus the control group. Low: compound 11 (50 mg/kg) + CCl₄; middle: compound 11 (100 mg/kg) + CCl₄; high: compound 11 (200 mg/kg) + CCl₄.

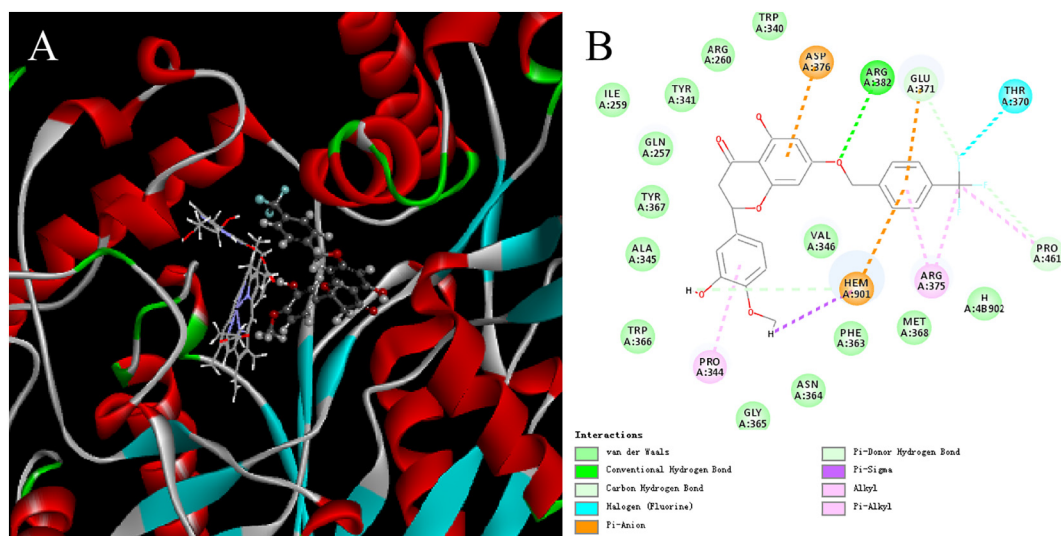


Fig. 5. Molecular docking study of 11 binding to iNOS protein. (A) Docking model of 11 in the active site of iNOS. (B) 2D interaction diagram of compound 11 and iNOS.

expression was reduced through NF- κ B signaling pathway, the quantity of iNOS expression after compound pre-treated was still high enough compared to vehicle. The significant NO inhibitory activities of the hesperetin derivatives prompted us to explore the interactions of these bioactive compounds with iNOS protein (PDB code: 3EAI) [27] by molecular docking studies using Discovery Studio 2017 R2. The results were unexpected and showed that the LibDockScore of the compounds were approximately in good accordance with the activity of NO inhibitory effects. As shown in Fig. 5, it revealed that compound 11 binds similarly in the iNOS active site heme pocket with the co-crystal

inhibitor ligand and showed a higher LibDockScore (175.714) than the co-crystal inhibitor (150.933). Additionally, the ether group of the hesperetin moiety established a conventional hydrogen bond with the hydroxyl group of the main chain of ARG382. It seemed that the presence of the 7-benzyl substituted hesperetin backbone led to the formation of the π -alkyl interaction with the amino acid residue PRO344, ARG375 and the π -anion interaction with the amino acid residue ASP376, HEM901, which were important to the binding site. The trifluoromethyl group established a π -donor hydrogen bond with GLU371, PRO461 and formed a halogen interaction with THR370. The results of

molecular docking indicate that the possible mechanism of NO inhibition of these bioactive hesperetin derivatives is to interact with the iNOS protein by targeting residues of the active cavities of iNOS. Further bioactive studies of the high LibDockScore compounds corresponding to the inflammatory activity are warranted, and further studies are currently underway in our laboratory. It reminds us that the anti-inflammatory activity of hesperetin derivatives may be the result of a Multi-target effect.

3. Conclusion

In summary, a series of hesperetin derivatives were successfully synthesized with high overall yield (65–80%). Their anti-inflammatory activity was evaluated by inhibiting IL-1 β , IL-6 and production of NO in mouse RAW264.7 macrophages. Several compounds showed potent inhibitory activity toward LPS-induced NO production as well as similar inhibitory activity on IL-1 β and IL-6. Compound **11** and **2c** appeared to be most potent among the synthesized compounds. In addition, compound **11** significantly suppressed cytokines produced. The present study suggests that the suppression of iNOS and NF- κ B pathway is, at least in part, related to the inhibitory activity of these hesperetin derivatives. Besides, the results of molecular docking study verify the anti-inflammatory effect of compound **11** and may reveal the Multi-target effect of hesperetin derivatives. From the *in vivo* study, compound **11** had an anti-inflammatory effect in the CCL₄-induced acute liver injury model by inhibiting the expression of cytokines in serum, including IL-1 β and IL-6. Moreover, it was also observed that compound **11** attenuated the levels of ALT, AST and liver histopathologic changes. It shows a promising anti-inflammatory activity which could be beneficial for use in the treatment of inflammatory diseases. Based on the structure-activity relationship of above-mentioned derivatives, established in this study, electron-withdrawing group attached on the A ring was crucial for the needed biological activities.

4. Experimental section

4.1. Chemistry

Reagents and starting materials were obtained from commercial suppliers and were used without purification. The reactions were monitored by thin-layer chromatography (TLC) on precoated silica GF254 plates. Column chromatography was done on silica gel 200 (Sorbent technologies). ¹H and ¹³C NMR spectra were recorded on a Bruker AM-300 (300 MHz) spectrometer with CDCl₃ or DMSO-*d*₆ as the solvent and TMS as the internal standard. Mass spectra data was obtained on an Agilent 6220 Accurate-Mass time-of-flight liquid chromatography/mass spectrometer (TOF LC/MS). Chemical names were generated using ChemDraw Ultra (CambridgeSoft, version16.0). Melting points were measured on a XT-4 microscopic thermometer (Beijing Tech Instrument Co., Ltd., Beijing, China) without calibration. Chemical shifts were reported in parts per million (d) units relative to the solvent peak. The ¹H NMR data were reported as peak multiplicities: s for singlet; d for doublet; t for triplet; and m for multiplet. Coupling constants were recorded in hertz.

4.2. General method for the preparation of hesperetin derivatives

K₂CO₃ (172.76 mg, 1.25 mmol) and the appropriate substituted bromine (4–10 mmol) were added, under stirring, to a solution of hesperetin (604 mg, 2 mmol) in anhydrous DMF (15 mL). Another 1 mmol of K₂CO₃ was intermittently added to the solution to keep the pH as a weak alkaline. The mixture was reacted at room temperature for 4–6 h under atmospheric conditions. The progress of the reaction was monitored by TLC. The reaction mixture poured into ice cold water then acidified by dilute hydrochloric acid and extracted with ethyl acetate, then washed three times with saturated aqueous NaCl solution. After

drying with anhydrous sodium sulfate, the solution was filtered through absorbent cotton. The precipitate obtained by removing the solvent under reduced pressure was purified by column chromatography (SiO₂) using trichloromethane/petroleum ether (1:1–5) as eluent. The purified precipitate was recrystallized from dichloromethane/petroleum ether.

4.2.1. (S)-7-[(2-fluorobenzyl)oxy]-5-hydroxy-2-(3-hydroxy-4-methoxyphenyl)chroman-4-one (**1a**)

Synthesis of **1a** followed the general procedure in 72% yield as a white to off-white crystalline solid: mp: 159–163 °C; ¹H NMR (400 MHz, CDCl₃): δ 12.00 (s, 1H, 5-OH), 7.44 (td, *J* = 7.5, 1.7 Hz, 1H, ArH), 7.33 (ddd, *J* = 7.3, 5.3, 1.8 Hz, 1H, ArH), 7.17 (td, *J* = 7.5, 1.1 Hz, 1H, ArH), 7.12–7.06 (m, 1H, ArH), 7.04 (d, *J* = 2.1 Hz, 1H, 2'-H), 6.93 (dd, *J* = 8.3, 2.0 Hz, 1H, 6'-H), 6.88 (d, *J* = 8.3 Hz, 1H, 5'-H), 6.16 (d, *J* = 2.3 Hz, 1H, 8-H), 6.13 (d, *J* = 2.3 Hz, 1H, 6-H), 5.33 (dd, *J* = 12.9, 3.0 Hz, 1H, 2-H), 5.13 (s, 2H, ArCH₂O), 3.92 (s, 3H, OCH₃), 3.08 (dd, *J* = 17.2, 12.9 Hz, 1H, 3-H), 2.79 (dd, *J* = 17.2, 3.1 Hz, 1H, 3-H); TOF-HRMS: *m/z* [M + H]⁺ calcd for C₂₃H₂₀FO₆: 411.1238; found: 411.1240.

4.2.2. (S)-7-[(3-fluorobenzyl)oxy]-5-hydroxy-2-(3-hydroxy-4-methoxyphenyl)chroman-4-one (**1b**)

Synthesis of **1b** followed the general procedure in 75% yield as a faint yellow powder: mp: 149–155 °C; ¹H NMR (400 MHz, CDCl₃): δ 12.00 (s, 1H, 5-OH), 7.35 (td, *J* = 8.0, 5.8 Hz, 1H, ArH), 7.15 (dd, *J* = 7.6, 0.6 Hz, 1H, ArH), 7.13–7.08 (m, 1H, ArH), 7.06–6.99 (m, 2H, ArH, 2'-H), 6.92 (dd, *J* = 8.4, 1.9 Hz, 1H, 6'-H), 6.88 (d, *J* = 8.3 Hz, 1H, 5'-H), 6.12 (d, *J* = 2.3 Hz, 1H, 8-H), 6.10 (d, *J* = 2.3 Hz, 1H, 6-H), 5.33 (dd, *J* = 12.9, 3.0 Hz, 1H, 2-H), 5.06 (s, 2H, ArCH₂O), 3.92 (s, 3H, OCH₃), 3.08 (dd, *J* = 17.2, 12.9 Hz, 1H, 3-H), 2.79 (dd, *J* = 17.2, 3.1 Hz, 1H, 3-H); TOF-HRMS: *m/z* [M + H]⁺ calcd for C₂₃H₂₀FO₆: 411.1238; found: 411.1239.

4.2.3. (S)-7-[(4-fluorobenzyl)oxy]-5-hydroxy-2-(3-hydroxy-4-methoxyphenyl)chroman-4-one (**1c**)

Synthesis of **1c** followed the general procedure in 78% yield as a faint yellow crystalline solid: mp: 167–168 °C; ¹H NMR (400 MHz, CDCl₃): δ 12.00 (s, 1H, 5-OH), 7.40–7.33 (m, 2H, ArH), 7.10–7.05 (m, 2H), 7.04 (d, *J* = 2.1 Hz, 1H, 2'-H), 6.92 (dd, *J* = 8.4, 2.0 Hz, 1H, 6'-H), 6.88 (d, *J* = 8.3 Hz, 1H, 5'-H), 6.12 (d, *J* = 2.3 Hz, 1H, 8-H), 6.09 (d, *J* = 2.3 Hz, 1H, 6-H), 5.33 (dd, *J* = 12.9, 3.0 Hz, 1H, 2-H), 5.02 (s, 2H, ArCH₂O), 3.92 (s, 3H, OCH₃), 3.07 (dd, *J* = 17.2, 12.9 Hz, 1H, 3-H), 2.79 (dd, *J* = 17.2, 3.1 Hz, 1H, 3-H); TOF-HRMS: *m/z* [M + H]⁺ calcd for C₂₃H₂₀FO₆: 411.1238; found: 411.1235.

4.2.4. (S)-5-hydroxy-2-(3-hydroxy-4-methoxyphenyl)-7-[(2-methylbenzyl)oxy]chroman-4-one (**1d**)

Synthesis of **1d** followed the general procedure in 74% yield as an off-white powder: mp: 137–141 °C; ¹H NMR (400 MHz, CDCl₃): δ 12.01 (s, 1H, 5-OH), 7.38–7.33 (m, 1H, ArH), 7.29–7.24 (m, 1H, ArH), 7.24–7.19 (m, 2H, ArH), 7.05 (d, *J* = 2.1 Hz, 1H), 6.93 (dd, *J* = 8.4, 2.0 Hz, 1H, 6'-H), 6.88 (d, *J* = 8.3 Hz, 1H, 5'-H), 6.16 (d, *J* = 2.3 Hz, 1H, 8-H), 6.13 (d, *J* = 2.3 Hz, 1H, 6-H), 5.33 (dd, *J* = 12.9, 3.0 Hz, 1H, 2-H), 5.04 (s, 2H, ArCH₂O), 3.92 (s, 3H, OCH₃), 3.08 (dd, *J* = 17.2, 13.0 Hz, 1H, 3-H), 2.79 (dd, *J* = 17.2, 3.0 Hz, 1H, 3-H), 2.34 (s, 3H, ArCH₃); TOF-HRMS: *m/z* [M + H]⁺ calcd for C₂₄H₂₃O₆: 407.1489; found: 407.1494.

4.2.5. (S)-5-hydroxy-2-(3-hydroxy-4-methoxyphenyl)-7-[(3-methylbenzyl)oxy]chroman-4-one (**1e**)

Synthesis of **1e** followed the general procedure in 67% yield as a white fluffy solid: mp: 118–125 °C; ¹H NMR (400 MHz, CDCl₃): δ 12.00 (s, 1H, 5-OH), 7.29–7.24 (m, 1H, ArH), 7.21–7.12 (m, 3H, ArH), 7.04 (d, *J* = 2.0 Hz, 1H, 2'-H), 6.92 (dd, *J* = 8.5, 2.0 Hz, 1H, 6'-H), 6.88 (d, *J* = 8.3 Hz, 1H, 5'-H), 6.14 (d, *J* = 2.3 Hz, 1H, 8-H), 6.11 (d, *J* = 2.3 Hz, 1H, 6-H), 5.31 (dt, *J* = 5.1, 2.5 Hz, 1H, 2-H), 5.02 (s, 2H, ArCH₂O), 3.91 (s, 3H, OCH₃), 3.07 (dd, *J* = 17.2, 12.9 Hz, 1H, 3-H),

2.78 (dd, $J = 17.2, 3.1$ Hz, 1H, 3-H), 2.37 (s, 3H, ArCH₃); TOF-HRMS: m/z [M + H]⁺ calcd for C₂₄H₂₃O₆: 407.1489; found: 407.1497.

4.2.6. (S)-5-hydroxy-2-(3-hydroxy-4-methoxyphenyl)-7-[[4-methylbenzyl]oxy]chroman-4-one (1f)

Synthesis of **1f** followed the general procedure in 73% yield as a white fluffy solid: mp: 153–155 °C; ¹H NMR (400 MHz, CDCl₃): δ 12.00 (s, 1H, 5-OH), 7.27 (d, $J = 8.0$ Hz, 2H, ArH), 7.19 (d, $J = 7.8$ Hz, 2H, ArH), 7.04 (d, $J = 2.1$ Hz, 1H, 2'-H), 6.92 (dd, $J = 8.5, 2.2$ Hz, 1H, 6'-H), 6.87 (d, $J = 8.3$ Hz, 1H, 5'-H), 6.13 (d, $J = 2.3$ Hz, 1H, 8-H), 6.10 (d, $J = 2.3$ Hz, 1H, 6-H), 5.31 (dd, $J = 12.9, 3.0$ Hz, 1H, 2-H), 5.02 (s, 2H, ArCH₂O), 3.91 (s, 3H, OCH₃), 3.06 (dd, $J = 17.2, 12.9$ Hz, 1H, 3-H), 2.77 (dd, $J = 17.2, 3.1$ Hz, 1H, 3-H), 2.36 (s, 3H, ArCH₃); TOF-HRMS: m/z [M + H]⁺ calcd for C₂₄H₂₃O₆: 407.1489; found: 407.1492.

4.2.7. (S)-2-[[5-hydroxy-2-(3-hydroxy-4-methoxyphenyl)-4-oxochroman-7-yl]oxy]methylbenzonitrile (1g)

Synthesis of **1g** followed the general procedure in 65% yield as a white powder: mp: 173–178 °C; ¹H NMR (400 MHz, CDCl₃): δ 12.00 (s, 1H, 5-OH), 7.75–7.68 (m, 1H, ArH), 7.67–7.59 (m, 2H, ArH), 7.50–7.43 (m, 1H, ArH), 7.04 (d, $J = 2.1$ Hz, 1H, 2'-H), 6.93 (dd, $J = 8.5, 2.0$ Hz, 1H, 6'-H), 6.89 (d, $J = 8.3$ Hz, 1H, 5'-H), 6.16 (d, $J = 2.3$ Hz, 1H, 8-H), 6.14 (d, $J = 2.3$ Hz, 1H, 6-H), 5.34 (dd, $J = 12.9, 3.0$ Hz, 1H, 2-H), 5.26 (s, 2H, ArCH₂O), 3.92 (s, 3H, OCH₃), 3.09 (dd, $J = 17.2, 12.9$ Hz, 1H, 3-H), 2.80 (dd, $J = 17.2, 3.1$ Hz, 1H, 3-H); TOF-HRMS: m/z [M + H]⁺ calcd for C₂₄H₂₀NO₆: 418.1285; found: 418.1285.

4.2.8. (S)-3-[[5-hydroxy-2-(3-hydroxy-4-methoxyphenyl)-4-oxochroman-7-yl]oxy]methylbenzonitrile (1h)

Synthesis of **1h** followed the general procedure in 67% yield as an off-white powder: mp: 200–205 °C; ¹H NMR (400 MHz, [D₆]DMSO): δ 12.10 (s, 1H, 5-OH), 9.11 (s, 1H, 3'-OH), 7.91 (br, 1H, ArH), 7.83 (d, $J = 7.7$ Hz, 1H, ArH), 7.79 (d, $J = 7.9$ Hz, 1H, ArH), 7.63 (t, $J = 7.8$ Hz, 1H, ArH), 6.96–6.94 (m, 2H, 2'-H, 5'-H), 6.89 (dd, $J = 8.3, 2.1$ Hz, 1H, 6'-H), 6.22 (d, $J = 2.3$ Hz, 1H, 8-H), 6.20 (d, $J = 2.3$ Hz, 1H, 6-H), 5.50 (dd, $J = 12.4, 3.0$ Hz, 1H, 2-H), 5.25 (s, 2H, ArCH₂O), 3.79 (s, 3H, OCH₃), 3.28 (dd, $J = 17.2, 12.4$ Hz, 1H, 3-H), 2.77 (dd, $J = 17.2, 3.2$ Hz, 1H, 3-H); TOF-HRMS: m/z [M + H]⁺ calcd for C₂₄H₂₀NO₆: 418.1285; found: 418.1284.

4.2.9. (S)-4-[[5-hydroxy-2-(3-hydroxy-4-methoxyphenyl)-4-oxochroman-7-yl]oxy]methylbenzonitrile (1i)

Synthesis of **1i** followed the general procedure in 70% yield as a white crystalline solid: mp: 165–166 °C; ¹H NMR (400 MHz, CDCl₃): δ 12.00 (s, 1H, 5-OH), 7.70–7.66 (m, 2H, ArH), 7.52–7.47 (m, 2H, ArH), 7.04 (d, $J = 2.0$ Hz, 1H, 2'-H), 6.92 (dd, $J = 8.5, 1.9$ Hz, 1H, 6'-H), 6.88 (d, $J = 8.3$ Hz, 1H, 5'-H), 6.11 (d, $J = 2.3$ Hz, 1H, 8-H), 6.08 (d, $J = 2.3$ Hz, 1H, 6-H), 5.33 (dd, $J = 12.9, 3.0$ Hz, 1H, 2-H), 5.13 (s, 2H, ArCH₂O), 3.92 (s, 3H, OCH₃), 3.08 (dd, $J = 17.2, 12.9$ Hz, 1H, 3-H), 2.80 (dd, $J = 17.2, 3.1$ Hz, 1H, 3-H); TOF-HRMS: m/z [M + H]⁺ calcd for C₂₄H₂₀NO₆: 418.1285; found: 418.1287.

4.2.10. (S)-5-hydroxy-2-(3-hydroxy-4-methoxyphenyl)-7-[[2-(trifluoromethyl)benzyl]oxy]chroman-4-one (1j)

Synthesis of **1j** followed the general procedure in 80% yield as a faint yellow crystalline solid: mp: 129–131 °C; ¹H NMR (400 MHz, CDCl₃): δ 12.00 (s, 1H, 5-OH), 7.70 (d, $J = 7.8$ Hz, 1H, ArH), 7.66 (d, $J = 7.8$ Hz, 1H, ArH), 7.58 (t, $J = 7.6$ Hz, 1H, ArH), 7.45 (d, $J = 7.7$ Hz, 1H, ArH), 7.04 (d, $J = 2.1$ Hz, 1H, 2'-H), 6.93 (dd, $J = 8.4, 1.9$ Hz, 1H, 6'-H), 6.88 (d, $J = 8.3$ Hz, 1H, 5'-H), 6.14 (d, $J = 2.3$ Hz, 1H, 8-H), 6.12 (d, $J = 2.3$ Hz, 1H, 6-H), 5.33 (dd, $J = 13.0, 3.0$ Hz, 1H, 2-H), 5.27 (s, 2H, ArCH₂O), 3.92 (s, 3H, OCH₃), 3.08 (dd, $J = 17.2, 13.0$ Hz, 1H, 3-H), 2.79 (dd, $J = 17.2, 3.0$ Hz, 1H, 3-H); TOF-HRMS: m/z [M + H]⁺ calcd for C₂₄H₂₀F₃O₆: 461.1206; found: 461.1210.

4.2.11. (S)-5-hydroxy-2-(3-hydroxy-4-methoxyphenyl)-7-[[3-(trifluoromethyl)benzyl]oxy]chroman-4-one (1k)

Synthesis of **1k** followed the general procedure in 78% yield as a white fluffy solid: mp: 141–143 °C; ¹H NMR (400 MHz, CDCl₃): δ 12.01 (s, 1H, 5-OH), 7.68–7.48 (m, 4H, ArH), 7.04 (d, $J = 2.1$ Hz, 1H, 2'-H), 6.93 (dd, $J = 8.4, 1.9$ Hz, 1H, 6'-H), 6.88 (d, $J = 8.3$ Hz, 1H, 5'-H), 6.14 (d, $J = 2.3$ Hz, 1H, 8-H), 6.11 (d, $J = 2.3$ Hz, 1H, 6-H), 5.34 (dd, $J = 12.9, 3.0$ Hz, 1H, 2-H), 5.11 (s, 2H, ArCH₂O), 3.92 (s, 3H, OCH₃), 3.08 (dd, $J = 17.2, 12.9$ Hz, 1H, 3-H), 2.80 (dd, $J = 17.2, 3.1$ Hz, 1H, 3-H); TOF-HRMS: m/z [M + H]⁺ calcd for C₂₄H₂₀F₃O₆: 461.1206; found: 461.1210.

4.2.12. (S)-5-hydroxy-2-(3-hydroxy-4-methoxyphenyl)-7-[[4-(trifluoromethyl)benzyl]oxy]chroman-4-one (1l)

Synthesis of **1l** followed the general procedure in 77% yield as a white powder: mp: 141–146 °C; ¹H NMR (400 MHz, CDCl₃): δ 12.01 (s, 1H, 5-OH), 7.65 (d, $J = 8.1$ Hz, 2H, ArH), 7.50 (d, $J = 8.0$ Hz, 2H, ArH), 7.04 (d, $J = 2.0$ Hz, 1H, 2'-H), 6.92 (dd, $J = 8.4, 2.0$ Hz, 1H, 6'-H), 6.88 (d, $J = 8.3$ Hz, 1H, 5'-H), 6.12 (d, $J = 2.3$ Hz, 1H, 8-H), 6.10 (d, $J = 2.3$ Hz, 1H, 6-H), 5.33 (dd, $J = 12.9, 3.0$ Hz, 1H, 2-H), 5.13 (s, 2H, ArCH₂O), 3.91 (s, 3H, OCH₃), 3.08 (dd, $J = 17.2, 12.9$ Hz, 1H, 3-H), 2.79 (dd, $J = 17.2, 3.1$ Hz, 1H, 3-H); TOF-HRMS: m/z [M + H]⁺ calcd for C₂₄H₂₀F₃O₆: 461.1206; found: 461.1210.

4.2.13. (S)-7-(benzyloxy)-5-hydroxy-2-(3-hydroxy-4-methoxyphenyl)chroman-4-one (1m)

Synthesis of **1m** followed the general procedure in 71% yield as a white fluffy solid: mp: 142–144 °C; ¹H NMR (400 MHz, CDCl₃): δ 12.00 (s, 1H, 5-OH), 7.41–7.30 (m, 5H, ArH), 7.04 (d, $J = 2.1$ Hz, 1H, 2'-H), 6.92 (dd, $J = 8.5, 2.2$ Hz, 1H, 6'-H), 6.88 (d, $J = 8.3$ Hz, 1H, 5'-H), 6.14 (d, $J = 2.3$ Hz, 1H, 8-H), 6.11 (d, $J = 2.3$ Hz, 1H, 6-H), 5.32 (dd, $J = 12.9, 3.0$ Hz, 1H, 2-H), 5.07 (s, 2H, ArCH₂O), 3.91 (s, 3H, OCH₃), 3.07 (dd, $J = 17.2, 12.9$ Hz, 1H, 3-H), 2.78 (dd, $J = 17.2, 3.1$ Hz, 1H, 3-H); TOF-HRMS: m/z [M + H]⁺ calcd for C₂₃H₂₁O₆: 393.1333; found: 393.1331.

4.2.14. (S)-7-ethoxy-5-hydroxy-2-(3-hydroxy-4-methoxyphenyl)chroman-4-one (2a)

Synthesis of **2a** followed the general procedure in 66% yield as a white fragmentary solid: mp: 145–151 °C; ¹H NMR (400 MHz, CDCl₃): δ 12.00 (s, 1H, 5-OH), 7.04 (d, $J = 2.1$ Hz, 1H, 2'-H), 6.93 (dd, $J = 8.2, 1.9$ Hz, 1H, 5'-H), 6.88 (d, $J = 8.3$ Hz, 1H, 4'-H), 6.05 (d, $J = 2.3$ Hz, 1H, 8-H), 6.03 (d, $J = 2.3$ Hz, 1H, 6-H), 5.32 (dd, $J = 12.9, 3.0$ Hz, 1H, 2-H), 4.04 (q, $J = 7.0$ Hz, 2H, O), 4.04 (q, $J = 7.0$ Hz, 2H, OCH₂C), 3.92 (s, 3H, OCH₃), 3.07 (dd, $J = 17.2, 12.9$ Hz, 1H, 3-H), 2.78 (dd, $J = 17.1, 3.1$ Hz, 1H, 3-H), 1.40 (t, $J = 7.0$ Hz, 3H, OCCH₃); TOF-HRMS: m/z [M + H]⁺ calcd for C₁₈H₁₉O₆: 331.1176; found: 331.1178.

4.2.15. (S)-5-hydroxy-2-(3-hydroxy-4-methoxyphenyl)-7-propoxychroman-4-one (2b)

Synthesis of **2b** followed the general procedure in 75% yield as a yellow crystalline solid: mp: 129–130 °C; ¹H NMR (400 MHz, CDCl₃): δ 12.00 (s, 1H, 5-OH), 7.04 (d, $J = 2.1$ Hz, 1H, 2'-H), 6.93 (dd, $J = 8.4, 2.0$ Hz, 1H, 5'-H), 6.88 (d, $J = 8.3$ Hz, 1H, 4'-H), 6.05 (d, $J = 2.3$ Hz, 1H, 8-H), 6.03 (d, $J = 2.3$ Hz, 1H, 6-H), 5.32 (dd, $J = 12.9, 3.0$ Hz, 1H, 2-H), 3.92 (t, $J = 6.6$ Hz, 2H, OCH₂), 3.91 (s, 3H, OCH₃), 3.06 (dd, $J = 17.2, 12.9$ Hz, 1H, 3-H), 2.78 (dd, $J = 17.1, 3.1$ Hz, 1H, 3-H), 1.84–1.73 (m, 2H, OCCH₂C), 1.01 (t, $J = 7.4$ Hz, 3H, OCCH₃); TOF-HRMS: m/z [M + H]⁺ calcd for C₁₉H₂₁O₆: 345.1333; found: 345.1331.

4.2.16. (S)-7-(allyloxy)-5-hydroxy-2-(3-hydroxy-4-methoxyphenyl)chroman-4-one (2c)

Synthesis of **2c** followed the general procedure in 65% yield as an off-white crystalline solid: mp: 130–135 °C; ¹H NMR (400 MHz, CDCl₃): δ 12.00 (s, 1H, 5-OH), 7.04 (d, $J = 2.1$ Hz, 1H, 2'-H), 6.93 (dd, $J = 8.3, 2.1$ Hz, 1H, 6'-H), 6.88 (d, $J = 8.3$ Hz, 5H, 5'-H), 6.07 (d, $J = 2.3$ Hz,

1H, 8-H), 6.05 (d, $J = 2.3$ Hz, 1H, 6-H), 6.04–5.95 (m, 1H, OCCH=C), 5.40 (do, $J = 17.3$, 1.6 Hz, 1H, OCC=CH), 5.35–5.28 (m, 2H, OCC=CH, 2-H), 4.54 (dt, $J = 5.3$, 1.5 Hz, 2H, OCH₂C=C), 3.92 (s, 3H, OCH₃), 3.07 (dd, $J = 17.2$, 12.9 Hz, 1H, 3-H), 2.78 (dd, $J = 17.2$, 3.1 Hz, 1H, 3-H); TOF-HRMS: m/z [M + H]⁺ calcd for C₁₉H₁₉O₆: 343.1176; found: 343.1174.

4.3. Biological assays and experimental procedures

4.3.1. Animal and treatment

C57BL/6 mice (weighting about 18–22 g each) were obtained from the Experimental Animal Center, Anhui Medical University. All the animal experimental and procedures were approved by the Ethic Committee and the Animal Experimental Committee of Anhui Medical University. Mice were reviewed and performed under the permission of the Animal Experiments Guidelines and Animal Care of Chinese Academy of Sciences. The mice were housed in micro isolator cages and received food and water *ad libitum*. For all experiments, C57BL/6 mice were randomly divided into six groups ($n = 8$ per group): normal group, model group, compound 11 treatment group (50 mg/kg, 100 mg/kg, 200 mg/kg) [28], and Silymarin group (200 mg/kg) [29]. Compound 11 treatment group, CCl₄ group and Silymarin group were injected intraperitoneally with 1% CCl₄ dissolved in olive oil (10 ml/kg in oil) to induce acute liver injury model [30], in addition, compound 11 treatment groups and Silymarin group were given *via* gavage different concentrations of compound 11 and Silymarin at the same volume for 7 days before. Compounds dissolved in 0.5% sodium carboxymethyl cellulose (CMC-Na) distilled water solution for gavage administration. Control group was given *via* gavage for 0.5% CMC-Na only and injected intraperitoneally the same volume of vehicle (olive oil). Mouse serum was collected stored at -80°C for the detection of inflammatory factors. The biggest lobe of the liver was excised and sectioned from each C57BL/6 mice and fixed with 4% paraformaldehyde for at least 24 h then embedded in paraffin. The pathological changes of liver was observed and photographed by Olympus BX-51 microscope after 4 μm thick sections stained with hematoxylin and eosin (H & E) with a standard procedure.

4.3.2. Cell culture

RAW 264.7 cells, purchased from Cell Bank of Chinese Academy of Sciences (Shanghai, China), were cultured in DMEM (Cyclone, USA), supplemented with 10% fetal bovine serum (Gibson), 100 units/mL of penicillin (Bigtime, China), 100 mg/mL of streptomycin (Bigtime, China). Cell cultures were maintained at 37°C in a humidified atmosphere containing 5% CO₂.

4.3.3. MTT cytotoxicity assay and cell viability

Cytotoxicity and cell viability was determined by 3-(4, 5-dimethylthiazol-2-yl)-2, 5-diphenyltetrazolium bromide (MTT, Sigma, USA) assay. Briefly, cells were inoculated at a density of 5×10^3 cells/well into 96-well plate and cultured at 37°C for 12 h. Cultured cells were treated with vehicle (control) and various concentrations of compound for 24 h. After incubation, 20 μL MTT solution (5 mg/mL in PBS) was added to each well and incubated for another 4 h. Media were removed and dimethyl sulfoxide (DMSO) was added to dissolve purple crystals. Then the absorbance at 490 nm was measured using a microplate reader (Synergy HTX, Biotec, USA). The values (IC₅₀) were calculated by SPSS 16.0. The cell viability was calculated from the plotted results using untreated cells at 100%.

4.3.4. Measurement of NO levels

NO has a short half-life and is oxidized to stable nitrite. Consequently, to evaluate the inhibitory activity of the test compounds on LPS-induced NO production, RAW 264.7 cells were plated at a density of 2×10^5 per well in a 6-well culture plate and incubated in a 37°C humidified incubator (5% CO₂) for 12 h. Then the media were

replaced and cells were then incubated with or without 1 $\mu\text{g}/\text{mL}$ LPS in the presence or absence of the test compounds (10 μM) for 24 h. The supernatant were collected and stored at -80°C prior to analysis. The amount of nitrite released in the culture supernatant was measured using the Gris reagent (0.1% naphthylethylenediamine and 1% sulfanilamide in 5% H₃PO₄ solution, Bigtime). Nitrite levels in the samples were calculated from a standard curve with a known concentration of sodium nitrite, and the absorbance of the samples was then measured at 540 nm using a microplate reader.

4.3.5. Measurement of cytokines

The cell culture supernatants were collected and the IL-1 β and IL-6 levels were determined by enzyme-linked immunosorbent assay (ELISA) (Ela science, China) following the manufacturer's protocol. The IL-1 β and IL-6 levels in Mouse serum were measured by the same method. Two independent experiments were performed in triplicate and a representative set of data (means \pm standard deviations) was used to determine the activity of each compound. The absorbance of the samples was then measured at 450 nm using a microplate reader. The inhibition rate of each production was calculated as inhibition rate (%) = $[1 - (\text{sample optical density} - \text{blank optical density}) / (\text{control optical density} - \text{blank optical density})] \times 100$.

4.3.6. ALT/AST activity assay

Serum extracted from C57BL/6 mice was stored at -80°C . The serum levels of Alanine aminotransferase (ALT) and Aspartate aminotransferase (AST) were assayed by using ALT and AST activity assay kits (Jincheng, Wuhan, China). The absorbance at 510 nm was obtained with a microplate reader.

4.3.7. Western blot analysis

After culture supernatants were harvested, cells were collected and lysed with RIPA lysis buffer (Bigtime, China). Cell lysates were centrifuged at 1.2 k rpm for 30 min at 4°C . The protein concentrations in cell lysates were determined by using the BCA protein assay kit (Bigtime, China). Equal amounts of protein were separated using SDS-PAGE. Proteins were transferred to PVDF membranes (Millipore, USA) and subsequently blocked in 5% skim milk in Tries-buffered saline (TBS, Booster, China) containing 1% tween 20 for 1 h at room temperature. After incubation with the appropriate primary antibody for a night, membranes were incubated for 1 h at room temperature with a secondary antibody (ZSGB-BIO, China). Following three washes in TBST, immunoreactivity bands were visualized using the ECL-chemiluminescent kit (ECL-plus, Thermo Scientific). Primary antibodies used were: iNOS, I κ B α , p65 and p-p65 from Abcam and actin from ZSGB-BIO.

4.4. Molecular docking

To explore the potential interacting mode of the isolated compounds with the iNOS protein (PDB code: 3EAI) [27], a molecular modeling study was performed using the docking program named Lib Dock, a software package in Discovery Studio 2017 R2. The molecular docking procedure was performed to eliminate any bond length and bond angle biases, so the ligands (compounds 1a–1m and 2a–2c) were subjected to a full minimization prior to docking. The binding affinities (LibDock-Score) in Discovery Studio 2017 R2 were used to evaluate the interactions between iNOS and the ligands. The standard 3D structures of all compounds for molecular docking were constructed by ChemDrew 16.0 software.

4.5. Statistical analysis

All experiments were repeated at least three times. Data are presented as the means \pm standard deviation (SD) for the indicated number of independently performed experiments. The significance of

differences between drug-treated groups compared to vehicle was determined by one way ANOVA using SPSS v16.0. The difference was considered statistically significant when $p^{(*)} < 0.05$, $(**) < 0.01$, $(***) < 0.001$.

Conflict of interest statement

The authors declare no conflict of interest.

Acknowledgements

Financial support by the National Natural Science Foundation of China (No. 81473268), Higher Education Natural Science Foundation of Anhui Province (KJ2016A364) and National Students' project for innovation and entrepreneurship training program (201610366036) is gratefully acknowledged.

References

- [1] B. Li, A.L. Huang, Y.L. Zhang, et al., Design, synthesis and evaluation of Hesperetin derivatives as potential multifunctional anti-Alzheimer agents[J], *Molecules* 22 (7) (2017).
- [2] K.Y. Jung, J. Park, Y.S. Han, et al., Synthesis and biological evaluation of hesperetin derivatives as agents inducing apoptosis[J], *Bioorg. Med. Chem.* 25 (1) (2017) 397–407.
- [3] W. Luo, Y. Chen, T. Wang, et al., Design, synthesis and evaluation of novel 7-aminoalkyl-substituted flavonoid derivatives with improved cholinesterase inhibitory activities[J], *Bioorg. Med. Chem.* 24 (4) (2016) 672–680.
- [4] M.P. Corcoran, D.L. Mckay, J.B. Blumberg, Flavonoid basics: chemistry, sources, mechanisms of action, and safety[J], *J. Nutr. Gerontol. Geriatr.* 31 (3) (2012) 176–189.
- [5] B. Zhang, T. Chen, Z. Chen, et al., Synthesis and anti-hyperglycemic activity of hesperidin derivatives[J], *Bioorg. Med. Chem. Lett.* 22 (23) (2012) 7194–7197.
- [6] Q.Q. Wang, J.B. Shi, C. Chen, et al., Hesperetin derivatives: synthesis and anti-inflammatory activity[J], *Bioorg. Med. Chem. Lett.* 26 (5) (2016) 1460–1465.
- [7] E.E. Mulvihill, A.C. Burke, M.W. Huff, Citrus flavonoids as regulators of lipoprotein metabolism and atherosclerosis[J], *Annu. Rev. Nutr.* 36 (2016) 275–299.
- [8] A. Roohbakhsh, H. Parhiz, F. Soltani, et al., Molecular mechanisms behind the biological effects of hesperidin and hesperetin for the prevention of cancer and cardiovascular diseases[J], *Life Sci.* 124 (2015) 64–74.
- [9] A. Ahmadi, A. Shadboorestan, S.F. Nabavi, et al., The role of hesperidin in cell signal transduction pathway for the prevention or treatment of cancer[J], *Curr. Med. Chem.* 22 (30) (2015) 3462–3471.
- [10] H. Parhiz, A. Roohbakhsh, F. Soltani, et al., Antioxidant and anti-inflammatory properties of the citrus flavonoids hesperidin and hesperetin: an updated review of their molecular mechanisms and experimental models[J], *Phytother. Res.* 29 (3) (2015) 323–331.
- [11] M. Yamamoto, H. Jokura, K. Hashizume, et al., Hesperidin metabolite hesperetin-7-O-glucuronide, but not hesperetin-3'-O-glucuronide, exerts hypotensive, vasodilatory, and anti-inflammatory activities[J], *Food Funct.* 4 (9) (2013) 1346–1351.
- [12] T.K. Hoang, T.K. Huynh, Nguyen T.D. Synthesis, Characterization, anti-inflammatory and anti-proliferative activity against MCF-7 cells of O-alkyl and O-acyl flavonoid derivatives[J], *Bioorg. Chem.* 63 (2015) 45–52.
- [13] R. Li, L. Cai, D.Y. Ren, et al., Therapeutic effect of 7, 3'-dimethoxy hesperetin on adjuvant arthritis in rats through inhibiting JAK2-STAT3 signal pathway[J], *Int. Immunopharmacol.* 14 (2) (2012) 157–163.
- [14] X. Lin, L.N. Kong, C. Huang, et al., Hesperetin derivative-7 inhibits PDGF-BB-induced hepatic stellate cell activation and proliferation by targeting Wnt/beta-catenin pathway[J], *Int. Immunopharmacol.* 25 (2) (2015) 311–320.
- [15] W.X. Li, X. Chen, Y. Yang, et al., Hesperetin derivative-11 suppress hepatic stellate cell activation and proliferation by targeting PTEN/AKT pathway[J], *Toxicology* 381 (2017) 75–86.
- [16] W.J. Jiang, K. Ishiuchi, M. Furukawa, et al., Stereospecific inhibition of nitric oxide production in macrophage cells by flavanols: synthesis and the structure-activity relationship[J], *Bioorg. Med. Chem.* 23 (21) (2015) 6922–6929.
- [17] A.H. Abdelazeem, S.I. Khan, S.W. White, et al., Design, synthesis and biological evaluation of bivalent benzoxazolone and benzothiazolone ligands as potential anti-inflammatory/analgesic agents[J], *Bioorg. Med. Chem.* 23 (13) (2015) 3248–3259.
- [18] V. Kondyliis, S. Kumari, K. Vlantis, et al., The Interplay of IKK, NF-kappaB and RIPK1 Signaling in the Regulation of Cell Death, Tissue Homeostasis and Inflammation[J], *277(1)* (2017), pp. 113–127.
- [19] G.M. Sundaram, P. Veera Bramhachari, Molecular interplay of pro-inflammatory transcription factors and non-coding RNAs in esophageal squamous cell carcinoma [J], *Immunol. Rev.* 39 (6) (2017) 1010428317705760.
- [20] J.A. Roman-Blas, S.A. Jimenez, NF-kappaB as a potential therapeutic target in osteoarthritis and rheumatoid arthritis[J], *Osteoarthr. Cartil.* 14 (9) (2006) 839–848.
- [21] W.J. Jiang, A. Daikonya, M. Ohkawara, et al., Structure-activity relationship of the inhibitory effects of flavonoids on nitric oxide production in RAW264.7 cells[J], *Bioorg. Med. Chem.* 25 (2) (2017) 779–788.
- [22] D.H. Bach, J.Y. Liu, W.K. Kim, et al., Synthesis and biological activity of new phthalimides as potential anti-inflammatory agents[J], *Bioorg. Med. Chem.* 25 (13) (2017) 3396–3405.
- [23] P. Mandrekar, D. Catalano, G. Szabo, Inhibition of lipopolysaccharide-mediated NFkappaB activation by ethanol in human monocytes[J], *Int. Immunol.* 11 (11) (1999) 1781–1790.
- [24] J. Wu, Y. Zhang, Y. Cai, et al., Discovery and evaluation of piperid-4-one-containing mono-carbonyl analogs of curcumin as anti-inflammatory agents[J], *Bioorg. Med. Chem.* 21 (11) (2013) 3058–3065.
- [25] L. Li, Y.F. Zhou, Y.L. Li, et al., In vitro and in vivo antioxidative and hepatoprotective activity of aqueous extract of Cortex Dictamni[J], *World J. Gastroenterol.* 23 (16) (2017) 2912–2927.
- [26] N.B. Qin, S.G. Li, X.Y. Yang, et al., Bioactive terpenoids from *Silybum marianum* and their suppression on NO release in LPS-induced BV-2 cells and interaction with iNOS[J], *Bioorg. Med. Chem. Lett.* 27 (10) (2017) 2161–2165.
- [27] G.Y. Xia, T. Yao, B.Y. Zhang, et al., Withapubesides A-D: natural inducible nitric oxide synthase (iNOS) inhibitors from *Physalis pubescens*[J], *Org. Biomol. Chem.* 15 (47) (2017) 10016–10023.
- [28] X. Chen, H.W. Ding, H.D. Li, et al., Hesperetin derivative-14 alleviates inflammation by activating PPAR-gamma in mice with CCl4-induced acute liver injury and LPS-treated RAW264.7 cells[J], *Toxicol. Lett.* 274 (2017) 51–63.
- [29] J.C. Tsai, C.S. Chiu, Y.C. Chen, et al., Hepatoprotective effect of *Coreopsis tinctoria* flowers against carbon tetrachloride-induced liver damage in mice[J], *BMC Complement. Altern. Med.* 17 (1) (2017) 139.
- [30] H.W. Ding, A.L. Huang, Y.L. Zhang, et al., Design, synthesis and biological evaluation of hesperetin derivatives as potent anti-inflammatory agent[J], *Fitoterapia* 121 (2017) 212–222.